Encyclopedia of Earthquake Engineering
DOI 10.1007/978-3-642-36197-5_290-1

Non-Double-Couple Earthquakes

G. R. Foulger* and Bruce R. Julian
Department of Geological Sciences, Durham University, Durham, UK

Introduction

Non-double-couple ("non-DC") earthquake mechanisms differ from what is expected for pure shear faulting in a homogeneous, isotropic, elastic medium. Until the mid-1980s, the DC assumption underlay nearly all seismological analysis, and was highly successful in advancing our understanding of tectonic processes and of seismology in general. In recent years, though, many earthquakes have been found that do not fit the DC model. Earthquakes that depart strongly from DC theory range in size over many orders of magnitude and occur in many environments, but are particularly common in volcanic and geothermal areas. Moreover, minor departures from the DC model are detected increasingly frequently in studies using high-quality data. These observations probably reflect departures from idealized models, caused by effects such as rock anisotropy or fault curvature.

At the same time, it has become clear that industrial activities such as oil and gas production and storage, hydrofracturing, geothermal energy exploitation, CO_2 sequestration, and waste disposal can induce earthquakes, and that these events often have non-DC mechanisms. Induced earthquakes pose legal hazards because of their destructive potential, but they can also be beneficial, because they can be used to monitoring physical processes that accompany industrial activity.

Non-DC earthquakes are therefore important for improving our understanding of how faults and volcanoes work, perhaps leading some day to an ability to predict earthquakes and eruptions, for avoiding nuisance seismicity in connection with industrial activity, and for monitoring such activity in detail.

Non-DC earthquake mechanisms, by definition, require for their description a more general mathematical formalism than the DC model. The most widely used such formalism is the expansion of the elastodynamic field in terms of the spatial moments of the equivalent-force system (Gilbert 1970). Usually, attention is restricted to second moments, and thus to second-rank moment tensors, and moreover these tensors are usually assumed to be symmetric, so that they have six independent components (A DC has four independent components.). This restriction is not always justified, however. Sources involving net forces or torques are theoretically possible, and phenomena such as landslides and volcanic eruptions provide clear examples of them.

Because it has two extra adjustable parameters, a moment tensor can describe volume changes and general kinds of shear deformation. This increased generality allows the moment tensor to encompass physical processes such as geometrically complex faulting, tensile faulting, faulting in anisotropic media, faulting in heterogeneous media (e.g., near an interface), and polymorphic phase transformations.

The moment tensor also has an important computational property: Mathematical expressions for static and dynamic displacement fields are linear in the moment-tensor components. This property facilitates the evaluation of these fields and enormously simplifies the inverse problem of deducing source mechanisms from observations.

*Email: G.R.Foulger@durham.ac.uk

Encyclopedia of Earthquake Engineering
DOI 10.1007/978-3-642-36197-5_290-1

Representation of Earthquake Mechanisms

The Equivalent Force System

Physically, an earthquake involves a nonlinear failure process occurring within a limited region. The equivalent force system, acting in an intact (unfaulted) "model" medium, would produce the same displacement field outside the source region. Any physical source has a unique equivalent force system in a given model medium, but the converse statement is not true. Different physical processes can have identical force systems and therefore identical static and dynamic displacement fields.

The equivalent force system is all that can be deduced from observations of displacement fields, so it constitutes a phenomenological description of the source. There is a one-to-one correspondence between equivalent force systems and elastodynamic fields outside the source region, so we can, in principle at least, determine force systems from observations. On the other hand, the correspondence between force systems and physical source processes is one-to-many, so equivalent force systems (and therefore seismic and geodetic observations) cannot uniquely diagnose physical source processes.

Failure can be regarded as a sudden localized change in the constitutive relation (stress–strain law) in the Earth (Backus 1977). Before an earthquake, the stress field satisfies the equations of equilibrium. At the time of failure, a rapid change in the constitutive relation causes the stress field to change. The resulting disequilibrium causes dynamic motions that radiate elastic waves. We disregard the effect of gravity in the following discussion. In the absence of external forces, the equation of motion is

$$\rho \ddot{u}_i = \sigma_{ij,j}, \tag{1}$$

where $\rho(\mathbf{x})$ is density, $\mathbf{u}(\mathbf{x}, t)$ is the particle displacement vector, $\sigma(\mathbf{x}, t)$ is the physical stress tensor, $\mathbf{x}$ is position, and t is time. Dots indicate differentiation with respect to t, ordinary subscripts indicate Cartesian components of vectors or tensors, the subscript $,j$ indicates differentiation with respect to the jth Cartesian spatial coordinate x_j, and duplicated indices indicate summation. The true stress is unknown, however, so in theoretical calculations we use the stress $\mathbf{s}(\mathbf{x}, t)$, given by the constitutive law of the model medium (usually Hooke's law). If we replace σ_{ij} by s_{ij} in the equations of motion, though, we must also introduce a correction term, $\mathbf{f}(\mathbf{x}, t)$:

$$\rho \ddot{u}_i = s_{ij,j} + f_i, \tag{2}$$

$$f_i \stackrel{\text{def}}{=} \left(\sigma_{ij} - s_{ij}\right)_{,j}. \tag{3}$$

This term has the form of a body-force density and is the equivalent force system of the earthquake. It differs from zero only within the source region.

Net Forces and Torques

Nearly all analyses of earthquake source mechanisms explicitly exclude net forces and torques. The equivalent forces given by Eq. 3, which arise from the imbalance between true physical stresses and those in the model, are consistent with these restrictions. The stress glut $\sigma_{ij} - s_{ij}$ is symmetric, so $\mathbf{f}$ exerts no net torque at any point. Furthermore, $\sigma_{ij} - s_{ij}$ vanishes outside the source region, so Gauss's theorem implies that the total force vanishes at each instant.

More complete analysis, however, including the effects of gravitation and mass advection, shows that Eq. 3 is based on overly restrictive assumptions and that net force and torque components are possible for realistic sources within the Earth (Takei and Kumazawa 1994). These forces and torques transfer linear and angular momentum between the source region and the rest of the Earth, with both types of momentum

Encyclopedia of Earthquake Engineering
DOI 10.1007/978-3-642-36197-5_290-1

conserved for the entire Earth. An easily understood example is the collapse of a cavity, in which rocks fall from the ceiling to the floor. While the rocks are falling, the Earth outside the cavity experiences a net upward force, relative to the state before and after the event.

The net force component in any source is constrained by the principle of conservation of momentum; if the source region is at rest before and after the earthquake, the total impulse of the equivalent force (its time integral) must vanish. No such requirement holds for the torque. The total torque exerted by gravitational forces need not vanish even after the earthquake. Horizontal displacement of the center of mass of the source region leads to a gravitational torque, which must be balanced by stresses on the boundary of the source and causes the radiation of elastic waves. Because gravity acts vertically, there can be no net torque about a vertical axis.

The Moment Tensor

We cannot use the equivalent force system $\mathbf{f}(\mathbf{x}, t)$ and the elastodynamic Eq. 2 to determine the displacement field for a hypothetical source. The equivalent force system itself depends on the displacement field that is being sought. Two different approaches are commonly used: (i) In the kinematic approach we assume some mathematically tractable displacement field in the source region (e.g., suddenly imposed slip, constant over a rectangular fault plane), derive the equivalent force system from Eq. 3, and solve Eq. 2 for the resulting displacement field outside the source region; and (ii) in the inverse approach, we use Eq. 2 to determine the force system $\mathbf{f}(\mathbf{x}, t)$ from the observed displacement field and compare the result with force systems predicted theoretically for hypothesized source processes. The most useful way to parameterize the force system in this approach is to use its spatial moments.

The Moment-Tensor Expansion for the Response

Given the equivalent force system $\mathbf{f}(\mathbf{x}, t)$, computing the response of the Earth is a linear problem, and its solution can be expressed as an integral over the source volume V (Aki and Richards 2002, Eq. 3.1, omitting displacement and traction discontinuities for simplicity):

$$u_i(\mathbf{x}, t) = \iiint_V G_{ij}(\mathbf{x}, \xi, t) * f_j(\xi, t) d^3\xi, \tag{4}$$

where $G_{ij}(\mathbf{x}, \xi, t)$ is the Green's function, which gives the ith component of displacement at position $\mathbf{x}$ and time t caused by an impulsive force in the j direction applied at position ξ and time 0, and the symbol * indicates temporal convolution. If we expand the Green's function in a Taylor series in the source position ξ,

$$G_{ij}(\mathbf{x}, \xi, t) = G_{ij}(\mathbf{x}, \mathbf{0}, t) + G_{ij,k}(\mathbf{x}, \mathbf{0}, t)\xi_k + \dots \ , \tag{5}$$

Eq. 4 for the response becomes

$$u_i(\mathbf{x}, t) = G_{ij}(\mathbf{x}, \mathbf{0}, t) * F_j(t) + G_{ij,k}(\mathbf{x}, \mathbf{0}, t) * M_{jk}(t) + \dots \ , \tag{6}$$

where

$$F_j(t) \stackrel{\text{def}}{=} \iiint_V f_j(\xi, t) d^3\xi \tag{7}$$

is the total force exerted by the source and

Encyclopedia of Earthquake Engineering
DOI 10.1007/978-3-642-36197-5_290-1

$$M_{jk}(t) \stackrel{\text{def}}{=} \iiint_V \xi_k f_j(\xi, t) d^3\xi \tag{8}$$

is the moment tensor. If the equivalent force is derivable from a stress glut via Eq. 3, then the moment tensor is the negative of the volume integral of the stress glut:

$$M_{jk}(t) = -\iiint_V \left(\sigma_{ij} - s_{ij}\right) d^3\xi \tag{9}$$

The moment tensor is a second-rank tensor, which describes a superposition of nine elementary force systems, with each component of the tensor giving the strength (moment) of one force system. The diagonal components M_{11}, M_{22}, and M_{33} correspond to linear dipoles that exert no torque, and the off-diagonal elements M_{12}, M_{13}, M_{21}, M_{23}, M_{31}, and M_{32} correspond to force couples. It is usually assumed that the moment tensor is symmetric, ($M_{12} = M_{21}$, $M_{13} = M_{31}$, $M_{23} = M_{32}$), so that the force couples exert no net torque (see above), in which case only six moment-tensor components are independent. In this case, the off-diagonal components correspond to three pairs of force couples, each exerting no net torque ("double couples").

The magnitudes of the six (or nine) elementary force systems (the moment-tensor components) transform according to standard tensor laws under rotations of the coordinate system, so there exist many different combinations of elementary forces that are equivalent. In particular, for a symmetric (six-element) moment tensor one can always choose a coordinate system in which the force system consists of three orthogonal linear dipoles, so that the moment tensor is diagonal. In other words, a general point source can be described by three values (the principal moments) that describe its physics and three values that specify its orientation.

The moment tensor has three important properties that make it useful for representing seismic sources. (1) It makes the "forward problem" of computing theoretical seismic-wave excitation linear. A general source is represented as a weighted sum of elementary force systems, so any seismic wave is just the same weighted sum of the waves excited by the elementary sources. The linearity of the forward problem in turn makes much more tractable the inverse problem of determining source mechanisms from observations. (2) It simplifies the computation of wave excitation. By transforming the moment tensor into an appropriately oriented coordinate system, the angles defining the observation direction can be made to take on special values such as 0 and $\pi/2$. Thus radiation by the elementary sources must be computed not for a general direction, but for only a few directions for which the computation is easier. In a laterally homogeneous medium, for example, radiation must be computed for only a single azimuth. (3) The moment tensor is more general than the DC representation. It includes DCs as special cases, but has two more free parameters than a DC (six vs. four), which enable it to represent sources involving volume changes and more general types of shear.

Higher-Rank Moment Tensors

As Eq. 6 shows, "the" moment tensor described above is only one of an infinite sequence of spatial moments that appear in the expansion of the Earth's response to an earthquake. The later terms involve higher-rank moment tensors, which contain information about the spatial and temporal distribution of failure in an earthquake, and have great potential value for studying source finiteness and rupture propagation.

Encyclopedia of Earthquake Engineering
DOI 10.1007/978-3-642-36197-5_290-1

Surface Sources (Faults)

A fault is a surface across which there is a discontinuity in displacement. The equivalent force distribution, **f**, for a generally oriented fault in an elastic medium is, from Eq. 2,

$$f_k(\eta, t) = -\iint_A [u_i(\xi, t)] c_{ijkl} \nu_j \frac{\partial}{\partial \eta l} \delta(\eta - \xi) dA, \tag{10}$$

where η is the position where the force is evaluated, ξ is the position of the element of area dA, and the integration extends over the fault surface (Aki and Richards 2002, Eq. 3.5). The unit vector normal to the fault surface is $\nu(\xi)$ and $[\mathbf{u}(\xi, t)]$ is the displacement discontinuity across the fault in the direction of ν. The components of the elastic modulus tensor are c_{ijkl} and $\delta(\mathbf{x})$ is the three-dimensional Dirac delta function.

Substituting the force distribution from Eq. 10 into Eq. 8 gives the moment tensor of a general fault,

$$M_{ij} = -c_{ijkl} A \overline{\nu_k [u_l]}, \tag{11}$$

where A is the total fault area and the overbar indicates the average value over the fault.

Shear Faults

For a planar shear fault (with normal ν in the x_3 direction and displacement discontinuity $[\mathbf{u}]$ in the x_1 direction, say, so that $\nu_1 = \nu_2 = 0$ and $[u_2] = [u_3] = 0$) in a homogeneous isotropic medium ($c_{ijkl} = \lambda\delta_{ij}\delta_{km}\delta_{lm} + 2\mu\delta_{ik}\delta_{jl}$), Eq. 8 gives a moment tensor with two nonzero components $M_{13} = M_{31} = \mu A\overline{u}$, where $\bar{u}$ is the average slip. This corresponds to a pair of force couples, one with forces in the x_1 direction and moment arm in the x_3 direction, and the other with these directions interchanged.

We get the same DC moment tensor for a fault with normal in the x_1 direction and displacement discontinuity in the x_3 direction. This ambiguity between “conjugate” faults is an example of the fundamental limitations on the information that can be deduced from equivalent force systems.

Tensile Faults

For a tensile fault in a homogeneous isotropic medium, with the fault lying in the x_1-x_2 plane and opening in the x_3 direction, $\nu_1 = \nu_2 = 0$ and $[u_1] = [u_2] = 0$. Equation 8 gives a moment tensor with three non-zero components: $M_{11} = M_{22} = \lambda A\overline{u}$ and $M_{33} = (\lambda + 2\mu)A\overline{u}$, corresponding to two dipoles in the fault plane with moments of $\lambda A\bar{u}$, and a third dipole oriented normal to the fault and with a moment of $(\lambda + 2\mu)A\overline{u}$.

Volume Sources

Some possible non-DC source processes, such as polymorphic phase transformation, occur throughout a finite volume rather than on a surface. The equivalent force system often can be expressed in terms of the “stress-free strain” $\Delta_\sigma e_{ij}$, which is the strain that would occur in the source volume if the tractions on its boundary were held constant by externally applied artificial forces (It might more accurately be called the “fixed-stress strain.”). By reasoning that involves a sequence of imaginary cutting, straining, and welding operations (e.g., Aki and Richards 2002, Sect. 3.4), the moment tensor of such a volume source is found to be

$$M_{ij} = \iiint_V c_{ijkl} \Delta_\sigma e_{kl} dV. \tag{12}$$

DOI 10.1007/978-3-642-36197-5_290-1

For a stress-free volume change $\Delta_\sigma V$ in an isotropic medium, for example,

$$M_{ij} = K\Delta_\sigma V\delta_{ij}, \tag{13}$$

where $K = \lambda + (2/3)\mu$ is the bulk modulus.

The stress-free strain is *not*, in general, the strain that actually occurs in a seismic event (Richards and Kim 2005). Because the source is imbedded in the Earth, its deformation is resisted by the stiffness of the surrounding medium, making the true strain changes smaller than the stress-free values. For example, in terms of the true volume change ΔV_t, the moment tensor of an isotropic source in an infinite isotropic elastic medium is

$$M_{ij} = (\lambda + 2\mu)\Delta_t V\delta_{ij}, \tag{14}$$

so

$$\Delta_t V = \frac{\lambda + (2/3)\mu}{\lambda + 2\mu}\Delta_\sigma V. \tag{15}$$

The distinction is quantitatively significant; for an infinite homogeneous Poisson solid, $\Delta_t V = (5/9)\ \Delta_\sigma V$. Furthermore, the stiffness seen by the source, and thus the true strain, depends on the elasticity structure outside the source volume.

Decomposing Moment Tensors

To make a general moment tensor easier to understand, it helps to decompose it into simpler force systems. First, we express the moment tensor in its principal axis coordinate system. Three values (the Euler angles, for example) are needed to specify the orientation of this system, and three other values specify the moments of three orthogonal dipoles oriented parallel to the coordinate axes. Writing these three principal moments as a column vector, we first decompose the moment tensor into an isotropic force system and a deviatoric remainder,

$$\begin{bmatrix} M_1 \\ M_2 \\ M_3 \end{bmatrix} = M^{(V)} \begin{bmatrix} 1 \\ 1 \\ 1 \end{bmatrix} + \begin{bmatrix} M_1' \\ M_2' \\ M_3' \end{bmatrix}, \tag{16}$$

with $M^{(V)} \overset{\text{def}}{=} (M_1 + M_2 + M_3)/3$, and then decompose the deviatoric part into a DC (principal moments in the ratio $1 : -1 : 0$) and a "compensated linear vector dipole" (CLVD), a source with principal moments in the ratio $1 : -{}^1/_2 : -{}^1/_2$ (Knopoff and Randall 1970). Figure 1 illustrates the three elementary force systems used in this decomposition, showing their compressional-wave radiation patterns and the distributions of compressional-wave polarities on the focal sphere (an imaginary sphere surrounding the earthquake hypocenter, to which observations are often referred). Many other decompositions of the deviatoric part are possible, including many decompositions into two DCs or into two CLVDs. The method of Knopoff and Randall (1970), which makes the largest axis of the CLVD coincide with the corresponding axis of the DC, avoids pathological behavior and is the method most widely used in seismological research:

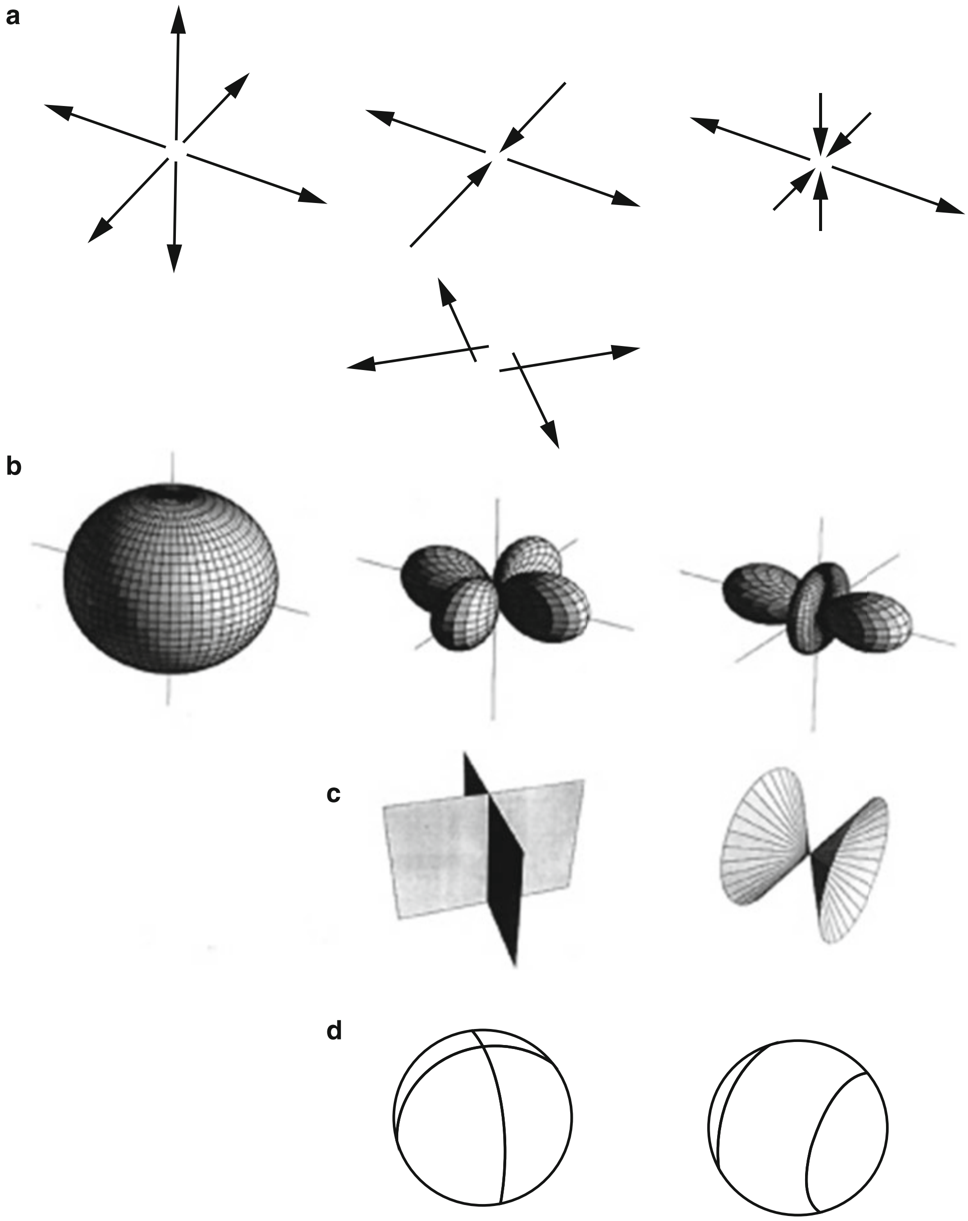

Fig. 1 Three source types commonly used in decomposing moment tensors: (from *left* to *right*) isotropic, double couple (DC), and compensated linear-vector dipole (CLVD). *Top row*: equivalent force systems, in principal-axis coordinates. For the DC, the force system in a fault-oriented coordinate system is shown underneath. *Second row*: compressional-wave radiation patterns. *Third row*: compressional-wave nodal surfaces. *Fourth row*: curves of intersection of nodal surfaces with the focal sphere

$$\begin{bmatrix} M_1' \\ M_2' \\ M_3' \end{bmatrix} = M^{(DC)} \begin{bmatrix} 0 \\ -1 \\ 1 \end{bmatrix} + M^{(CLVD)} \begin{bmatrix} -1/2 \\ -1/2 \\ 1 \end{bmatrix}, \tag{17}$$

with $M^{(DC)} = M_1' - M_2'$, and $M^{(CLVD)} = -2M_1'$. The moment-tensor elements are arranged so that $|M_1'| \leq |M_2'| \leq |M_3'|$.

The quantity

Encyclopedia of Earthquake Engineering
DOI 10.1007/978-3-642-36197-5_290-1

$$\varepsilon \stackrel{\text{def}}{=} \frac{-M'_1}{|M'_3|} \equiv \frac{1}{2} \frac{M^{(CLVD)}}{\left|M^{(DC)} + M^{(CLVD)}\right|} \tag{18}$$

is sometimes used as a measure of the departure of the deviatoric part of a moment tensor from a pure DC. It ranges in value from zero for a pure DC to $\pm^1/_2$ for a pure CLVD. Positive ε corresponds to extensional polarity for the major dipole of the CLVD component.

Displaying Focal Mechanisms

Focal-Sphere Polarity Plots

Since the 1960s, common practice has been to display DC mechanisms by showing the compressional-wave polarity fields on maps of a focal hemisphere, and this method is now also widely used for general symmetric moment tensors. Both azimuthal-equal-area (Lambert) and stereographic projections are used, with teleseismic data usually plotted on lower hemispheres and local data on upper hemispheres. Shaded fields usually represent positive polarities (outward first motions). Figures 2, 4, 6, 8, 9, 11, 12, and 13 below contain examples of focal-sphere polarity plots.

A disadvantage of focal-sphere polarity plots is that different mechanisms can lead to identical plots. Figure 2 shows, for example, that a rather wide range of mechanisms can have positive (or negative) compressional-wave polarities over the entire focal sphere.

Source-Type Plots

Focal-sphere polarity plots display information about source orientation as well as "source type" (the relative values of the principal moments). In fact, conventional DC polarity plots contain information about *only* source orientation. When considering non-DC mechanisms, however, it is useful to display the source type without regard to orientation. The normalized principal moments contain two independent degrees of freedom, and there are many possible ways to display such information in two dimensions. Figure 2 shows the "source-type plot" (Hudson et al. 1989), which gives $T \stackrel{\text{def}}{=} -2\varepsilon$ (Eq. 18) vs.

$$k \stackrel{\text{def}}{=} \frac{M^{(V)}}{\left|M^{(V)}\right| + \left|M'_3\right|}, \tag{19}$$

a measure of the volume change.

Determining Earthquake Mechanisms

Many types of seismic and geodetic data can be used to determine earthquake focal mechanisms. These range from simple polarities (signs) of observable quantities, through measurements of their amplitudes, to complete time histories of their evolution.

Wave Polarities

First-Motion Methods

P-phase polarities are the most commonly used data in focal-mechanism studies, because they can be determined easily, even using recordings of low dynamic range and accuracy from single-component seismometers. Such polarities alone are of very limited use, however, for studying (or even for

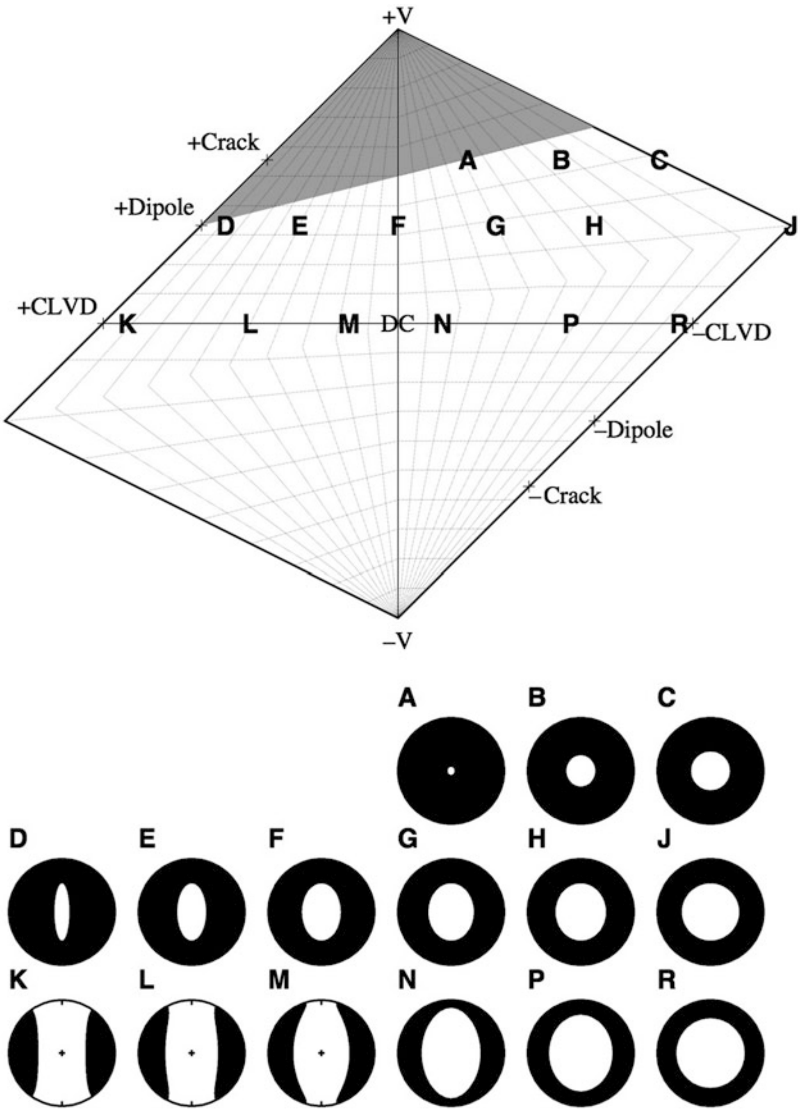

Fig. 2 *Top*: "Source-type plot" of Hudson et al. (1989), which displays earthquake mechanisms (symmetric moment tensors) without regard to their orientations. The quantity k (Eq. 19), which measures volume change, ranges from -1 at the *bottom* of the plot to +1 at the *top*, and is constant along the sub-horizontal grid lines. The quantity -2ε (Eq. 18), which describes the deviatoric part of the moment tensor, ranges from -1 on the *left-hand side* of the plot to +1 on the *right-hand side*, and is constant along the grid lines that run from *top* to *bottom*. DC: double-couple mechanisms; +Crack: Opening tensile faults; +Dipole: Force dipoles with forces directed outward; +CLVD: "Compensated linear-vector dipoles," with dominant dipoles directed outward. −Crack, −Dipole, and −CLVD: The same mechanisms with opposite polarities. *Shaded area*: Region in which all compressional waves have outward polarities. A similar region of inward polarities occurs at the *bottom* of the plot. *A–R*: Some representative mechanisms. *Bottom*: Conventional equal-area focal-hemisphere plots of compressional-wave polarities for 15 representative mechanisms shown on the source-type plot

identifying) non-DC earthquakes. Even with observations well distributed on the focal sphere, it usually is difficult to rule out DC mechanisms in practice. This difficulty is especially severe if the earthquake lacks a large isotropic component.

In analyzing *P*-wave polarities, seismologists usually constrain earthquake mechanism to be DCs. Finding a DC mechanism amounts to finding two orthogonal nodal planes (great circles on the focal sphere) that separate the compressional and dilatational polarities into four equal quadrants. Three independent quantities (fault-plane strike and dip angles and the rake angle of the slip vector, say) are needed to specify the orientations of the nodal planes. Nodal planes can be sought either manually, by plotting data on maps of the focal sphere and using graphical methods to find suitable nodal planes, or by using computerized methods, most of which systematically search through the space of possible solutions.

Moment-Tensor Methods

For general moment-tensor mechanisms, hand-fitting mechanisms to observed polarities is impractical. The number of unknown parameters increases from three to five (the six moment tensor components, normalized in some arbitrary way), and furthermore the theoretical nodal surfaces become general ellipses, rather than great circles, on the focal sphere. Searching methods still work, but the addition of two more unknown parameters makes them costly in terms of computer time. Linear programming (sections "Wave Amplitudes" and "Amplitude Ratios," below), an analytical method that treats linear inequalities, is well suited to determining moment tensors from observed wave polarities (Julian 1986).

Near-Field Polarities

Near-field observations (made within a few wavelengths of the source) provide a simple and elegant method of detecting an isotropic source component using a single radial-component seismogram (McGarr 1992). The method is not guaranteed to detect isotropic components whenever they exist, but it involves few assumptions, so detected isotropic components are comparatively reliable.

Assume that all the moment-tensor components are proportional to the unit step function, $U(t)$ (any monotonic function of time will work). Place the origin of the coordinate system at the source, with the x_1 axis directed toward the observer. Then from Eq. 4.29 of Aki and Richards (2002), in an infinite homogeneous medium the radial displacement (the x_1 component observed on the x_1 axis) is

$$u_1(t) = \frac{3}{4\pi\rho r^4}(3M_{11} - Tr\mathbf{M})w(t) \tag{20a}$$

$$+\frac{1}{4\pi\rho V_P^2 r^2}(4M_{11} - Tr\mathbf{M})U(t - r/V_P) \tag{20b}$$

$$-\frac{1}{4\pi\rho V_S^2 r^2}(3M_{11} - Tr\mathbf{M})U(t - r/V_S) \tag{20c}$$

$$+\frac{1}{4\pi\rho V_P^3 r}M_{11}\delta(t - r/V_P)\ , \tag{20d}$$

where

$$w(t) \stackrel{\text{def}}{=} \int_{r/V_P}^{r/V_S} \tau U(t - \tau)d\tau \tag{21}$$

vanishes for $t \le r/V_P$, increases monotonically for $r/V_P \le t \le r/V_S$, and is constant for $r/V_S \le t$. Here $r \equiv x_1$ is the source-observer distance and V_P and V_S are the compressional- and shear-wave speeds. The near-field term Eq. 20a produces a monotonic trend on the seismogram between the compressional and shear waves. For a purely deviatoric source ($Tr\,\mathbf{M} = 0$), the polarity of this near-field term must be the same as that of the compressional wave Eqs. 20b and 20d. Opposite polarities on any radial seismogram

Encyclopedia of Earthquake Engineering
DOI 10.1007/978-3-642-36197-5_290-1

imply that the source mechanism has an isotropic component. Similarly, the near-field shear wave Eq. 20c must have the opposite polarity to the compressional wave, and any observations to the contrary indicate an isotropic source component.

Polarities of Other Seismic Waves

The polarities of shear waves can furnish valuable information to complement compressional-wave first motions, but because shear seismic phases arrive later in the seismogram, where scattered energy ("signal-generated noise") is also arriving, their polarities often are difficult to measure reliably. An additional severe difficulty arises for vertically polarized shear (*SV*) waves incident at the surface beyond the critical angle $\sin^{-1}(V_S/V_P)$ (at epicentral distances between about 0.7 times the focal depth and several thousand kilometers). Outside the "shear-wave windows" at small and large distances, incident shear waves excite evanescent compressional waves that complicate signals and render them practically useless for analysis (Booth and Crampin 1985). Still another problem arises because wave scattering by heterogeneities near the surface excites compressional waves that arrive slightly before the direct shear wave, making the true S onset difficult to identify. These latter two difficulties are caused by conditions at or near the free surface and can be partially alleviated by installing seismometers in deep boreholes.

None of these problems affect horizontally polarized shear waves in spherically symmetric media, and in practice useful *SH* polarities can usually be determined reliably on transverse-component seismograms obtained by numerical rotation.

Wave Amplitudes

The amplitude of a radiated seismic wave contains far more information about the earthquake mechanism than does its polarity alone, so amplitude data can be valuable in studies of non-DC earthquakes. Moreover, because seismic-wave amplitudes are linear functions of the moment-tensor components, determining moment tensors from observed amplitudes is a linear inverse problem, which can be solved by standard methods such as least squares. Conventional least-squares methods, however, cannot invert polarity observations such as first motions, which typically are the most abundant data available. Linear programming methods, which can treat linear inequalities, are well suited to inverting observations that include both amplitudes and polarities (Julian 1986). In this approach, bounds are placed on observed amplitudes, so that they can be expressed as linear inequality constraints. Polarities are already in the form of linear inequality constraints if the moment-tensor representation is used.

Linear programming methods seek solutions by attempting to minimize the L1 norm (the sum of the absolute values) of the residuals between the constraints and the theoretical predictions.

Amplitude Ratios

Seismic-wave amplitudes are subject to distortion during propagation, particularly because of focusing and de-focusing by structural heterogeneities. A simple way to reduce the effect of this distortion when deriving earthquake mechanisms is to use as data the ratios of amplitudes of waves that have followed similar paths, such as *P*:*SV*, *P*:*SH*, or *SH* : *SV*. If the ratios of the wave speeds is constant in the Earth, then the amplitudes of the waves are affected similarly and the ratio is relatively unaffected.

Using amplitude ratios makes inverting for source mechanisms more difficult, however, because a ratio is a nonlinear function of its denominator. Systematic searching methods still work, but because the dimensionality of the model space is increased by two over that for a DC mechanism, the computational labor is greatly increased (typically by a factor of more than 100).

The efficient linear programming method described above is easily extended to treat amplitude-ratio data in addition to polarities and amplitudes (Julian and Foulger 1996). An observed ratio is expressed as a

Encyclopedia of Earthquake Engineering
DOI 10.1007/978-3-642-36197-5_290-1

pair of bounding values, each of which gives a linear inequality that is mathematically equivalent to a polarity observation with a suitably modified Green's function.

Waveforms

A digitized waveform is just a series of amplitude measurements, so waveform inversion may be regarded as an extension of amplitude inversion.

Mathematical Formulation

A theoretical seismogram can be written as a sum of terms, each of which is the temporal convolution of a Green's function and the time function of one source component (Eq. 6). The source components can include components of the equivalent force and moment-tensor components of any order. If there are n such source components (six, in the usual case of a symmetric second-rank moment tensor), which we arrange in a column vector $\phi(t)$, then a set of m seismograms corresponds to the system of simultaneous equations

$$\begin{bmatrix} u_1(t) \\ u_2(t) \\ \vdots \\ u_m(t) \end{bmatrix} = \begin{bmatrix} A_{11}(t) & \cdots & A_{1n}(t) \\ A_{12}(t) & \cdots & A_{2n}(t) \\ \vdots & \ddots & \vdots \\ A_{m1}(t) & \cdots & A_{mn}(t) \end{bmatrix} * \begin{bmatrix} \phi_1(t) \\ \phi_2(t) \\ \vdots \\ \phi_n(t) \end{bmatrix}, \tag{22}$$

where each matrix element A_{ij} is a Green's function giving the ith seismogram generated by a source whose jth component is the impulse $\delta(t)$, and whose other components are zero. The symbol * indicates temporal convolution. The Green's functions can be thought of as a multichannel filter, which takes the n source time functions $\phi_j(t)$ as inputs and generates as output the m synthetic seismograms $u_i(t)$.

Estimating the source time functions from a set of observed seismograms and assumed Green's functions is thus a multichannel inverse filtering, or deconvolution, problem. It can be solved, for example, by transforming to the frequency domain (so that the convolutions become multiplications) and then applying standard least-squares methods to solve for each spectral component. Alternatively, the output seismograms in Eq. 22 can be concatenated into a single time series, and the Green functions in each column of the matrix **A** similarly concatenated. Then, when each time series is expressed explicitly in terms of its samples, the least-squares normal equations turn out to have a "block-Toeplitz" structure, so that they can be solved efficiently by Levinson Recursion (Sipkin 1982).

Limitations

Imperfect Earth Models

If the Earth model used to analyze the radiation from an earthquake differs from the true structure of the Earth, systematic errors will be introduced into the Green functions and thus into inferred source mechanisms. Near-source anisotropy (section "Shear Faulting in an Anisotropic Medium") is one cause of such errors.

Deficient Combinations of Modes

Even if the Green's functions are correct, it may be impossible to determine the source mechanism completely in some circumstances. For particular types of seismic waves, there may be certain source characteristics that cannot be determined. For example, shear waves alone cannot detect isotropic source components, because purely isotropic sources do not excite shear waves. Similarly, sources with vertical symmetry axes (those whose only nonzero components are $M_{11} = M_{22}$ and M_{33}, with the x_3 axis vertical) excite no horizontally polarized shear (*SH*) or Love waves, and cannot be detected using such waves alone. For any Rayleigh mode, the component M_{33} occurs only in the combination $M_{11} + M_{22} + f(\omega)M_{33}$, where the frequency function $f(\omega)$ depends on the mode and the Earth model. The M_{33} component can be traded off against $M_{11} + M_{22}$ without changing this combination, so isotropic sources are unresolvable by Rayleigh waves of a single frequency and mode (Mendiguren 1977), and even with multimode observations, determining M_{33} requires a priori assumptions about its spectrum. In most studies, enough different modes and/or frequencies are used so that none of these degenerate situations arises. Furthermore, all general inversion methods in widespread use provide objective information about uncertainty and nonuniqueness in derived values, so degeneracies can be detected if they happen to occur.

Shallow Earthquakes

If an earthquake is effectively at the free surface (shallow compared to the seismic wavelengths used), then it is impossible to determine its full moment tensor. Only three moment-tensor components can be determined, and these are not enough even under the a priori assumption of a DC mechanism (which requires four parameters). This degeneracy follows from the proportionality between the coefficient C_{ij} giving the amplitude of a seismic mode excited by the moment-tensor component M_{ij} and the displacement derivative $u_{i,j}$ for the mode. (This proportionality follows from the principle of reciprocity.) Vanishing of the traction on the free surface,

$$\begin{aligned} \sigma_{13} &= \mu\left(u_{1,3} + u_{3,1}\right) = 0 \\ \sigma_{23} &= \mu\left(u_{2,3} + u_{3,2}\right) = 0 \\ \sigma_{33} &= \lambda\left(u_{1,1} + u_{2,2}\right) + (\lambda + 2\mu)u_{3,3} = 0, \end{aligned} \tag{23}$$

implies that three linear combinations of the excitation coefficients vanish:

$$\begin{gathered} C_{13} = 0 \\ C_{23} = 0 \\ \lambda C_{11} + \lambda C_{22} + (\lambda + 2\mu)C_{33} = 0. \end{gathered} \tag{24}$$

(Here we restrict ourselves to symmetric moment tensors.) Therefore a moment tensor whose only nonzero components are M_{13} and M_{23} radiates no seismic waves (to this order of approximation), and moreover a diagonal moment tensor with elements in the ratio $\lambda : \lambda : (\lambda + 2\mu)$ likewise radiates no seismic waves. The first case corresponds to a vertical dip-slip shear fault or a horizontal shear fault, and the second corresponds to a horizontal tensile fault. This second undeterminable source type has an isotropic component, so isotropic components cannot be determined for shallow sources.

This degeneracy is most often important in studies using surface waves or normal modes, because these are usually observed at frequencies below 0.05 Hz, for which the wavelengths are greater than the focal depths of many earthquakes.

Non-DC Earthquake Processes

Processes Involving Net Forces

Most experimental investigations of earthquake source mechanisms have excluded net forces and torques from consideration a priori. As discussed above in section "Net Forces and Torques," the laws of physics do not require such restrictions. Net forces are possible for an internal source because momentum can be

Encyclopedia of Earthquake Engineering
DOI 10.1007/978-3-642-36197-5_290-1

transferred between the source region and the rest of the Earth. Momentum conservation does, however, require that the impulse (time integral) of the net force component must vanish if the source is at rest before and after the event.

Landslides

Among sources that involve net forces, landslides have received the most attention. Modeling a landslide as a block of mass M sliding down a ramp gives an equivalent force of $-M\mathbf{a}$, where $\mathbf{a}$ is the acceleration of the block.

The gravitational forces on a landslide also produce a torque of magnitude $Mg\Delta x$, where g is the acceleration of gravity and Δx is the horizontal distance the slide travels.

Volcanic Eruptions

The eruption of material by a volcano applies a net force to the Earth, much as an upward-directed rocket exhaust would. Of course, the total impulse imparted to the Earth-atmosphere system is zero, as with any internal source, but the spatially and temporally concentrated force at the volcanic vent can generate observable seismic waves, whereas the balancing forces transmitted from the ejected material through the atmosphere back to the Earth's surface excite waves that probably are unobservable in practice. Therefore a volcanic eruption may be modeled as a point force $S\Delta P$, where S is the area of the vent and ΔP is the pressure difference between the source reservoir within the volcano and the atmosphere (Kanamori et al. 1984).

Other processes accompanying volcanic eruptions might act as seismic-wave sources. A change in pressure in a deep spherically symmetric reservoir acts as an isotropic source with a moment tensor given by Eq. 14 (section "Volume Sources"). For a tabular or crack-shaped reservoir, the force system is the same as that for a tensile fault, discussed in sections "Tensile Faults" and "Tensile Faulting."

Unsteady Fluid Flow

If the speed, and thus the momentum, of fluid flowing in a conduit varies with time, a time-varying net force,

$$\mathbf{F} = -\iiint_V \rho \mathbf{a} dV, \tag{25}$$

is exerted on the surrounding rocks, where ρ is the density of the fluid and $\mathbf{a}$ is its acceleration. This process may cause "long-period" volcanic earthquakes and the closely related phenomenon of volcanic tremor. Time variations in the flow speed might be caused by the breaking of barriers to flow, or be self-excited by nonlinear interaction between the flowing fluid and deformable channel walls (Julian 1994).

Complex Shear Faulting

Multiple Shear Events

If earthquakes occur close together in space and time, observed seismic waves may not be able to resolve them, and they may be misinterpreted as a single event. The apparent moment tensor of the composite event is then the sum of the true moment tensors of the earthquakes, and because the sum of two DCs is not, in general, a DC, shear faulting can produce non-DC mechanisms in this way. Combining DCs cannot ever produce mechanisms with isotropic (volume change) components, because the trace of the moment tensor is a linear function of its components, so multiple shear-faulting mechanisms lie on the horizontal axis of the source-type plot.

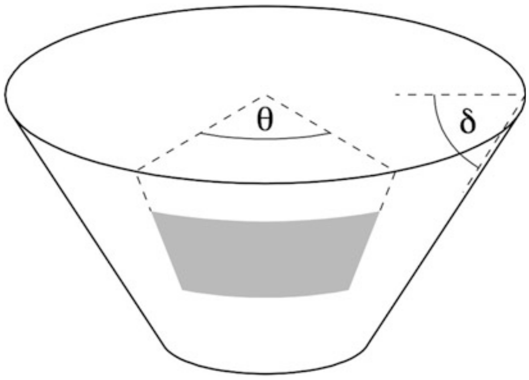

Fig. 3 Geometry of volcanic ring faulting used in computing mechanisms shown in Fig. 4. Dip-slip motion on fault of dip δ is uniformly distributed over azimuth range θ

By analyzing complete seismic waveforms, it is often possible to resolve a multiple event into subevents with different mechanisms. Doing this requires use of algorithms that allow the moment tensor to vary with time in a general way. Algorithms that assume that all the moment-tensor components have identical time functions can produce spurious non-DC mechanisms, even if the subevents have identical DC mechanisms.

Volcanic Ring Faults

Dikes intruded along conical surfaces with both outward and inward dips are often found in exhumed extinct volcanoes, and are expected consequences of the stresses caused by inflation and deflation of magma chambers (Anderson 1936). These dikes are of two types: “cone sheets,” which dip inward at about 30–70°, form as tensile faults during inflation, and nearly vertical or steeply outward-dipping “ring dikes” form through shear failure accommodating subsidence following deflation or eruption of magma. For both types, the axes of the cones are approximately vertical. If dip-slip shear faulting occurs on a conical fault, and the rupture in an earthquake spans a significant azimuth range (Fig. 3), the resulting mechanism, considered as a point source, can have a non-DC component (Ekström 1994). (Strike-slip motion on such a surface always gives pure DC mechanisms.) Figure 4 shows a suite of theoretical source mechanisms corresponding to dip-slip ruptures spanning various azimuth ranges on conical faults of different dips. For steeply dipping faults the non-DC components are small (for vertical faults they vanish), so cone sheets are more efficient than ring dikes as a non-DC process.

Tensile Faulting

Opening Tensile Faults in the Earth

An obvious candidate mechanism for geothermal and volcanic earthquakes is tensile faulting, in which the displacement discontinuity is normal, rather than parallel, to a fault surface. The equivalent force system of a tensile fault consists of three orthogonal linear dipoles with moments in the ratio $(\lambda + 2\mu):\lambda:\lambda$. It is equivalent to an isotropic source of moment $(\lambda + 2\mu/3)A\bar{u}$ plus a CLVD of moment $(4\mu/3)A\bar{u}$ (section “Tensile Faults”). The far-field compressional waves have all first motions outward, with amplitudes largest (by a factor of $1 + 2\mu/\lambda$) in the direction normal to the fault. Figure 2 shows the position of tensile faults on a source-type plot.

Compressive stress tends to prevent voids from forming at depth in the Earth, but high fluid pressure can overcome this effect and allow tensile failure to occur. The situation is conveniently analyzed using Mohr’s circle diagrams (Fig. 5). The effect of interstitial fluid at pressure p in a polycrystalline medium such as a rock is to lower the effective principal stresses by the amount p. Thus fluid pressure, if high

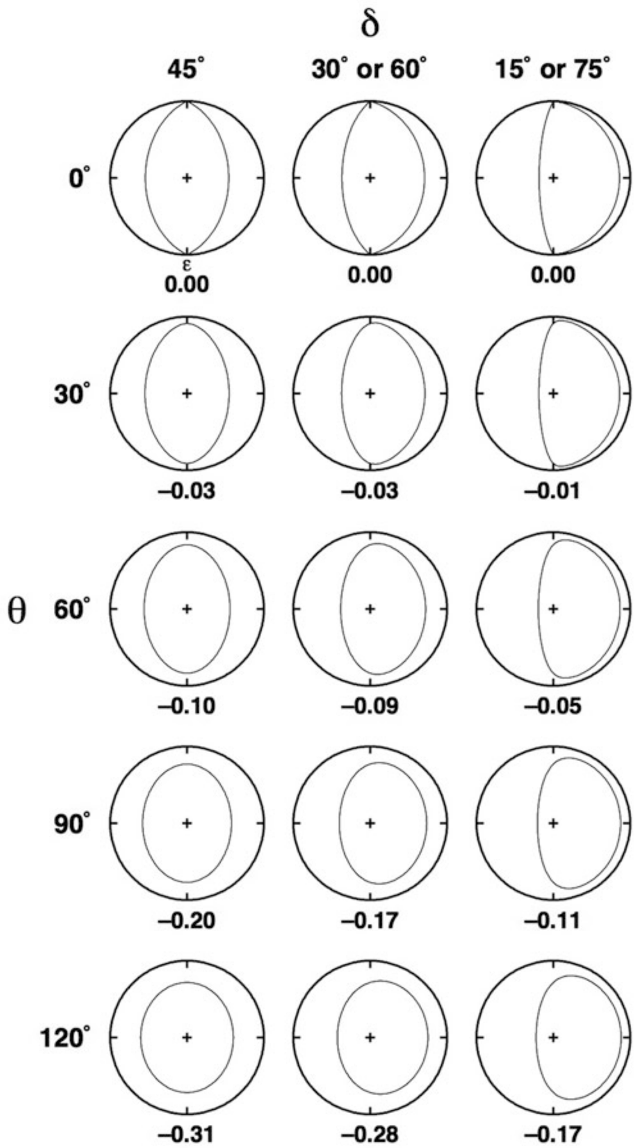

Fig. 4 Non-DC mechanisms for volcanic ring faulting (Fig. 3). Theoretical compressional-wave nodal surfaces for an arcuate dip-slip fault whose strike spans a range θ and averages north–south. Each focal sphere corresponds to two situations: a fault dipping to the west by the smaller angle δ given or to the east by the larger angle. All mechanisms are purely deviatoric. Numbers below each mechanism give values of ε (Eq. 18), which describe the deviatoric parts of the moment tensors. Upper focal hemispheres are shown in equal-area projection. Lower hemisphere plots are *left-right* mirror images. For normal faulting, central fields have dilatational polarity

enough, can cancel out much of the compressive stress caused by the overburden. Fluid pressures comparable to the lithostatic load are found surprisingly often in deep boreholes.

A second prerequisite for tensile failure is that the shear stresses be small, or equivalently that the principal stresses be nearly equal. The diameter of the Mohr's circle in Fig. 5 is equal to the maximum shear stress (difference between the extreme principal stresses). If this diameter is too large, the circle can touch the failure envelope only along its straight portion, which corresponds to shear failure. Only if the shear stress, and thus the diameter, is small will the circle first touch the failure envelope in the tensile field to the left of the τ axis.

DOI 10.1007/978-3-642-36197-5_290-1

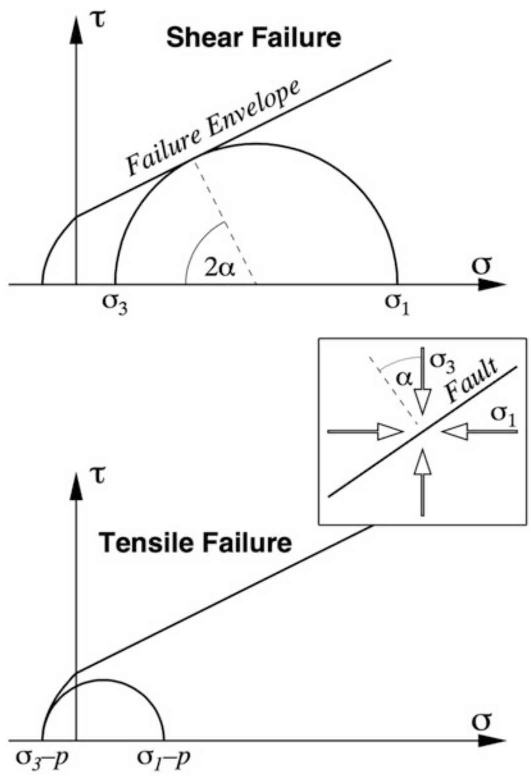

Fig. 5 Conditions for shear and tensile failure. Mohr's circle diagram shows the relationship between shear traction τ and normal traction σ across a plane in a stressed medium. Locus of (σ, τ) points for different orientations of the plane is a circle of diameter $\sigma_1 - \sigma_3$, centered at $((\sigma_1 + \sigma_3)/2)$, where σ_1 and σ_3 are the extreme principal stresses. Failure occurs when circle touches the "failure envelope," and the point of tangency determines the orientation of the resulting fault (see *inset*). (Theoretical failure envelope shown corresponds to Griffith theory of failure, as modified by F. A. McClintock and J. B. Walsh (Price 1966).) Straight portion of failure envelope in compressional field ($\sigma > 0$) represents the Navier-Coulomb criterion for shear failure. (*Top*) At high confining stress with no fluid pressure, only shear failure occurs. (*Bottom*) High fluid pressure lowers the effective confining stress, and tensile failure occurs for low stress differences

Combined Tensile and Shear Faulting

Although tensile faults could cause earthquakes that involve volume increases, they cannot explain non-DC earthquakes whose isotropic components indicate volume decreases. Tensile faults can open suddenly for a variety of reasons, but they would be expected to close gradually, and not to radiate elastic waves. If a tensile fault and a shear fault intersect, however, then stick–slip instability could cause sudden episodes of either opening or closing, with volume increases or decreases. The stresses around the tips of both shear and tensile faults favor this type of fault pairing, and faulting of this kind occurs in rocks in the laboratory (Brace et al. 1966). A similar situation can occur in the case of shear faulting near mines, with the tunnel playing the role of the tensile fault.

Figure 6 shows the theoretical source mechanisms for combined tensile and shear faults of different geometries and relative seismic moments. When the tensile fault opens or closes in the direction normal to its face, the mechanisms have large isotropic components, with most of the focal sphere having the same polarity as the tensile fault and two unconnected fields having the opposite polarity. The symmetry of the moment tensors makes it impossible to determine the angle between the two faults. An angle of $45° - \alpha$ is equivalent to an angle of $45° + \alpha$. When the tensile fault opens or closes obliquely, in the direction parallel to the shear fault, then the mechanisms are closer to DCs, and less sensitive to the relative seismic moments.

DOI 10.1007/978-3-642-36197-5_290-1

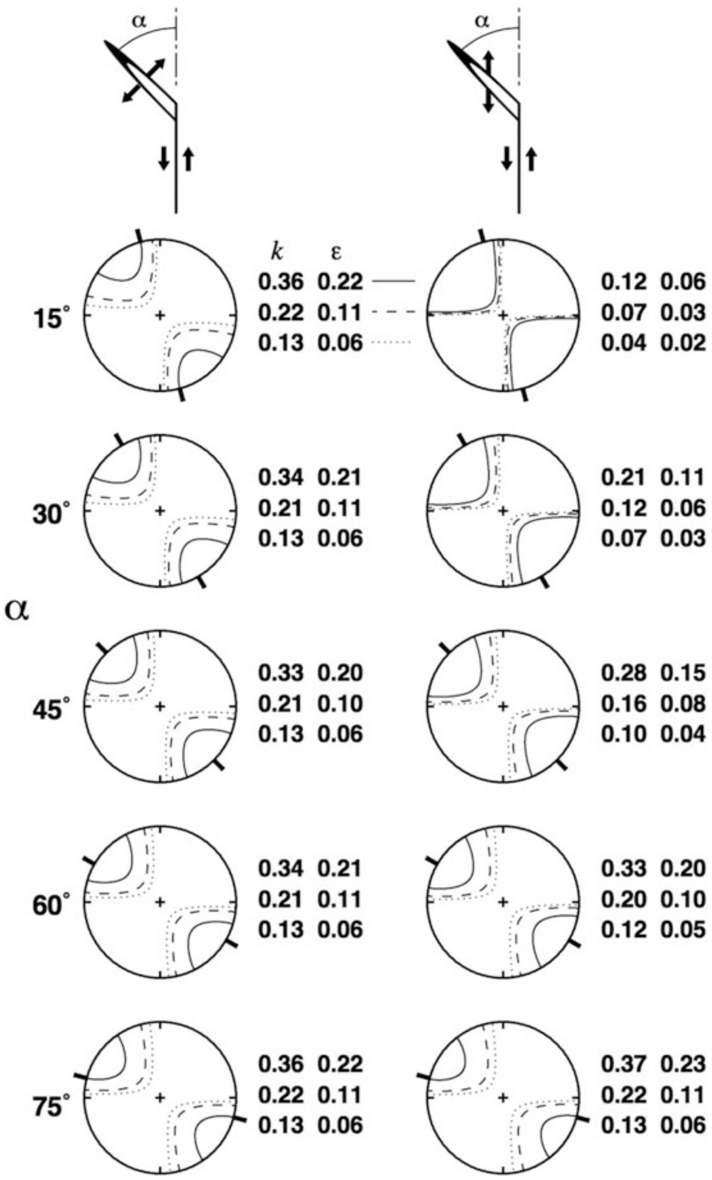

Fig. 6 Non-DC mechanisms for combined tensile and shear faulting with different geometries. Both faults are vertical, with the shear fault striking north–south and the tensile fault striking west of north at the angle α, indicated by bold ticks. *Left column*: tensile fault opening normal to its face. *Right column*: tensile fault opening obliquely, parallel to the shear fault. Compressional-wave nodal surfaces are shown for different relative moments of the tensile (M^T) and shear (M^S) components. *Solid curves*: $M^T = 0.5M^S$. *Dashed curves*: $M^T = 0.2M^S$. *Dotted curves*: $M^T = 0.1M^S$. Numbers to the *right* of each plot give values of k and ε (Eqs. 18 and 19), for each mechanism. Focal hemispheres (either upper or lower, because of symmetry) are shown in equal-area projection

If the dominant principal axis of the tensile fault lies in the same plane as the P and T axes of the shear fault (i.e., if the null axis of the shear fault lies in the tensile-fault plane), then the composite mechanism lies on the line between the DC and Crack positions on a focal-sphere plot. For more general (and less physically plausible) geometrical arrangements, the composite mechanism lies within a region consisting of two triangles (Fig. 7).

DOI 10.1007/978-3-642-36197-5_290-1

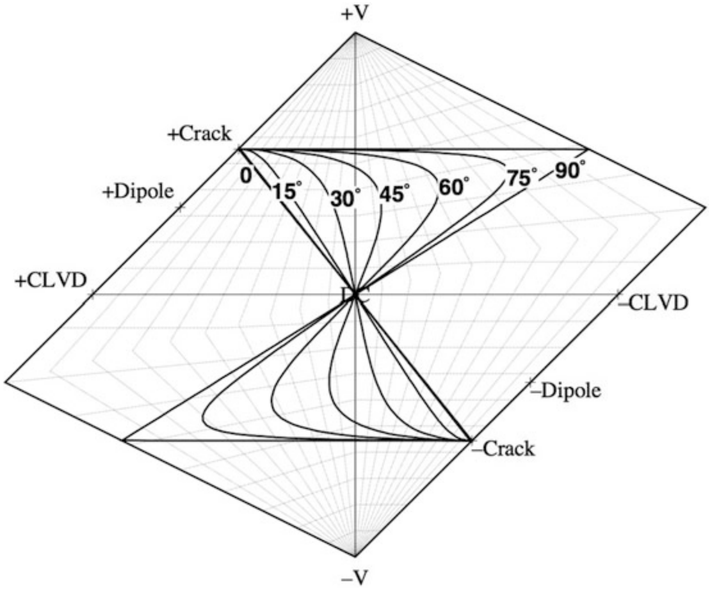

Fig. 7 Source types for combined tensile and shear faulting. Numbers give angles between the tensile-fault planes and the intermediate principal (null) axes of the shear faults. Small angles are physically most plausible (For the mechanisms shown in Fig. 6 this angle is zero.). For all possible relative orientations and moments, the source type lies between the corresponding curve and the *straight line* from +Crack to −Crack. The upper half of the plot corresponds to opening faults and the lower half to closing faults. For an explanation of the plotting method, see Fig. 2

Shear Faulting in an Anisotropic Medium

The equivalent force system of an earthquake depends on the constitutive law used to compute the model stress s_{ij} in Eq. 2. This means that a fault in an anisotropic elastic medium has a different equivalent force system than it would if the medium were isotropic, and in particular that a shear fault in an anisotropic medium generally has a non-DC moment tensor, which can be determined, for example, from Eq. 11 (Vavryčuk 2005). Most rocks are anisotropic, because of layering on a scale smaller than seismic wavelengths, preferential orientation of crystals, and the presence of cracks and inclusions, so most earthquakes are affected by anisotropy.

Elastic wave propagation in an anisotropic medium is more complicated in several ways than in an isotropic medium. The particle motion in body waves is no longer either longitudinal or transverse to the direction of propagation, but is generally oblique, so body-wave modes are referred to as “quasi-compressional” and “quasi-shear.” The “direction of propagation,” in fact is no longer a single direction, but rather two directions for each mode: the normal to the wavefront (the “phase velocity” direction) and the direction of energy transport (the “group velocity” direction, from the source to the observer).

Green’s functions for the anisotropic medium must be used to compute the radiated seismic waves for the force system given by Eq. 11 (Gajewski 1993) and to solve the inverse problem of determining the force system from observed seismograms. If enough information is available about source-region anisotropy to determine such Green’s functions, then it will be possible to recognize when non-DC force systems are consistent with shear faulting. In practice, however, information about anisotropy in earthquake focal regions is seldom available, so Green’s functions appropriate for isotropic constitutive laws are used instead. In this case, the non-DC force system of most interest is not the one given by Eq. 11, but rather the one that would be derived from seismic waves using an isotropic constitutive law when the focal region is actually anisotropic.

Encyclopedia of Earthquake Engineering
DOI 10.1007/978-3-642-36197-5_290-1

Shear Faulting in a Heterogeneous Medium

If an earthquake occurs in a place where the elastic moduli vary spatially, its apparent mechanism will be distorted, and a DC earthquake may appear to have non-DC components. This occurs when the spatial derivatives of Green's functions (strains) appearing in the second term on the right side of the moment expansion Eq. 6 vary significantly over the source region, so that the values at $\xi = 0$ are inappropriate for a portion of the moment release. In effect, neglected higher moments are contaminating estimates of the lower moments.

This effect is *not* a consequence of using an incorrect Earth model to compute the Green function. In this discussion, we assume that the Earth model and Green's function are exact. The distortion of the focal mechanism is caused by the finiteness of the source region. Errors in the Green function due to our incomplete knowledge of Earth structure and to the mathematical complexity of elastodynamics can cause severe errors in derived earthquake mechanisms, but that is a different phenomenon.

Consider an earthquake near an interface across which the elastic moduli change discontinuously (Woodhouse 1981), so that the truncated Taylor series Eq. 5 is a particularly poor approximation. Then the inferred mechanism of an earthquake that is assumed to occur on one side of the interface will be distorted if the earthquake actually is on the other side. If the source region includes both sides of the interface, it is unavoidable that a portion of the moment release will be distorted in this manner.

If we arrange the independent components of the moment tensor in a column vector,

$$\mathbf{m} \stackrel{\text{def}}{=} [M_{11}\ M_{12}\ M_{22}\ M_{13}\ M_{23}\ M_{33}]^T, \tag{26}$$

then the seismic waves excited can be written $\mathbf{g}^T\ \mathbf{m}$, where $\mathbf{g}$ is a column vector whose components are spatial derivatives of Green's functions appearing in the second term on the right side of Eq. 6. Because displacement and stress are continuous at the interface, the elements of $\mathbf{g}$ on one side of the interface are related to those on the other side by a relation that can be written

$$\mathbf{A}^+\mathbf{g}^+ = \mathbf{A}^-\mathbf{g}^-, \tag{27}$$

where $\mathbf{A}$ is a matrix that depends on the orientation of the interface and the elastic moduli adjacent to it, and the superscripts $^+$ and $^-$ indicate values on the two sides of the interface. It follows that

$$\mathbf{g}^{+T}\mathbf{m} = \mathbf{g}^{-T}\left[\mathbf{A}^{+-1}\mathbf{A}^-\right]^T\mathbf{m}, \tag{28}$$

or in other words that an earthquake with moment tensor $\mathbf{m}$ occurring on the $+$ side of the interface excites the same waves as an earthquake with moment tensor $[\mathbf{A}^{+-1}\mathbf{A}^-]^T\ \mathbf{m}$ occurring on the opposite $(-)$ side. In a coordinate system with the x_3 axis normal to the interface, the matrix connecting the true and apparent moment tensors is

$$\left[\mathbf{A}^{+-1}\mathbf{A}^-\right]^T = \begin{bmatrix} 1 & 0 & 0 & 0 & 0 & R_1 \\ 0 & 1 & 0 & 0 & 0 & 0 \\ 0 & 0 & 1 & 0 & 0 & 0 \\ 0 & 0 & 0 & R_2 & 0 & 0 \\ 0 & 0 & 0 & 0 & R_2 & 0 \\ 0 & 0 & 0 & 0 & 0 & R_3 \end{bmatrix}, \tag{29}$$

where

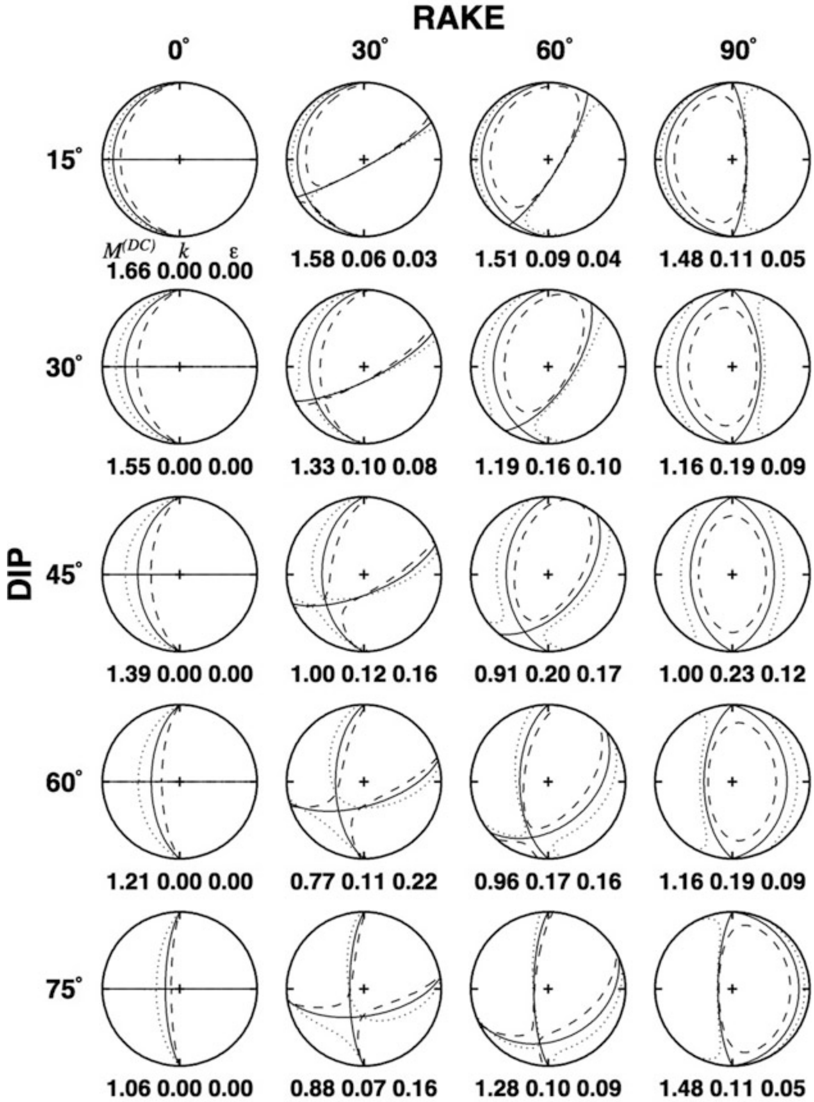

Fig. 8 Apparent non-DC mechanisms caused by shear faulting with unit moment near a horizontal interface, for various dip and rake angles. *Solid curves*: compressional-wave nodal planes corresponding to true (DC) mechanisms. *Dotted curves*: nodal surfaces for apparent mechanisms obtained if DC moment release on the low-speed side of interface is assumed to be on the high-speed side. *Dashed curves*: same, with sides interchanged. Both media are Poisson solids, and the ratio of elastic moduli across the interface is 1.7:1, corresponding to a wave-speed contrast of about 20 % if density is proportional to wave speed. Numbers below each mechanism give the DC moment and the values of k and ε (Eqs. 18 and 19) corresponding to the *dotted curves*. Dips of 0 are not shown because the apparent mechanisms are DCs (although with moments distorted by the ratio of the rigidity moduli). Dips of 90° correspond to cases with rake of 0 (first column). Focal hemispheres (which may be considered either upper or lower) are shown in equal-area projection

$$R_1 \stackrel{\text{def}}{=} \frac{\lambda^- - \lambda^+}{\lambda^+ + 2\mu^+}, \tag{30}$$

$$R_2 \stackrel{\text{def}}{=} \frac{\mu^-}{\mu^+}, \tag{31}$$

and

Encyclopedia of Earthquake Engineering
DOI 10.1007/978-3-642-36197-5_290-1

$$R_3 \stackrel{\text{def}}{=} \frac{\lambda^- + 2\mu^-}{\lambda^+ + 2\mu^+}. \tag{32}$$

Figure 8 shows the distortion of the apparent mechanisms of DCs of various orientations occurring adjacent to a horizontal interface across which the elastic-wave speeds change by 20 %. If the fault plane is parallel to the interface (or if the interface *is* the fault plane), then shear faulting does not lead to apparent non-DC mechanisms, although the scalar seismic moment is distorted. This case is not illustrated in the figure, but is clear from the structure of the matrix in Eq. 29. Only M_{13} and M_{23} are nonzero and matrix multiplication merely multiplies these elements by R_2, producing a DC of the same orientation, but with its moment multiplied by the contrast in rigidity modulus. If the fault is perpendicular to the interface, then the apparent mechanism is still a DC for all slip directions, but its orientation and seismic moment are distorted, as the first column of the figure illustrates. For general fault orientations, the apparent mechanism has artificial isotropic and CLVD components.

Rapid Polymorphic Phase Changes

Except in the shallow crust, compressional stresses in the Earth greatly exceed shear stresses. Therefore, earthquake processes that involve even relatively small volume changes could release large amounts of energy. For this reason, it has long been speculated that polymorphic phase transformations in minerals might cause deep earthquakes. Such speculation has been stimulated also by consideration of the simple theory of frictional sliding, which seems to require impossibly large shear tractions when the confining pressure is high, and by the theory of plate tectonics, which involves large-scale vertical motions in the upper mantle. Many common minerals undergo polymorphic changes in crystal structure in response to changes in pressure and temperature, and some of the major structural features in the Earth, most notably the "transition region" at depths between about 400 and 800 km in the upper mantle, are attributed to such phase changes (in this case, involving the mineral olivine, $(Fe, Mg)_2SiO_4$, transforming to the spinel and then perovskite crystal structures).

As slabs of lithosphere subduct into the mantle, olivine and other minerals are carried out of their stability fields and into the stability fields of denser phases, into which they transform. If these changes occur rapidly enough to radiate seismic waves, they constitute earthquakes, and their mechanisms will have isotropic components. They probably will also have deviatoric components, because the process of phase transformation will release shear strain, much as explosions are often observed to release tectonic shear strain. There seems to be no reason, however, why such a deviatoric component should be a DC rather than a CLVD, and in fact the CLVD force system was first invented as a possible mechanism for deep earthquakes caused by phase transformations (Knopoff and Randall 1970).

Observations

Non-DC earthquakes are observed in many environments, including volcanic and geothermal areas, mines, and deep subduction zones. They include both natural earthquakes and events induced by human activity. An in-depth review of many observed examples is given by Miller et al. (1998b).

Landslides and Volcanic Eruptions

Landslides and volcanic eruptions have equivalent force systems that include net forces (section "Landslides"). An example is the Mount St. Helens, Washington, eruption of May 18, 1980, which began with a landslide with a mass of about 5×10^{13} kg that traveled about 10 km from the volcano. The seismic

Encyclopedia of Earthquake Engineering
DOI 10.1007/978-3-642-36197-5_290-1

observations are well explained by two forces, a near-horizontal, southward directed force representing the landslide, and a vertical force representing the eruption (Kanamori et al. 1984).

The gravitational forces on a landslide also exert a torque, which can be substantial, on the source volume (section "Landslides"). The dimensions of the landslide that accompanied the May 18, 1980, eruption of Mt. St. Helens, for example, correspond to a net torque of about 5×10^{18} N m. By comparison, the two largest earthquakes accompanying the eruption had surface-wave magnitudes of about 5.3, which correspond to seismic moments of about 2.6×10^{17} N m. Apparently, no seismological analyses of landslides to date have included torques in the source mechanism.

Long-Period Volcanic Earthquakes

Long-period volcanic earthquakes have dominant seismic frequencies an order of magnitude lower than those of most earthquakes with comparable magnitudes. They are caused by unsteady flow of underground magmatic fluids and are expected to have mechanisms involving net forces (section "Unsteady Fluid Flow"). An example is a 33-km-deep, long-period earthquake that occurred a year before the 1986 eruption of Izu Ōshima volcano, Japan. The seismograms are characterized by nearly monochromatic shear-wave trains that have dominant frequencies of about 1 Hz and last for more than a minute. The shear-wave polarization directions are consistent with a net force mechanism.

Several types of non-DC earthquakes occur at the intensively monitored active Sakurajima volcano in southern Kyushu, Japan. It is a rich source of low-frequency earthquakes and explosion earthquakes, which accompany crater eruptions that radiate spectacular visible shock waves into the atmosphere. The moment tensors of the explosion earthquakes have been explained as either deflation of cracks or other cavities that might rapidly expel gas into the atmosphere (Uhira and Takeo 1994), or as sources dominated by vertical dipoles involving, for example, the opening of horizontal cracks (Iguchi 1994). The discrepancies between the results of these two studies reflect the difficulty of distinguishing between vertical forces and vertical dipoles.

Short-Period Volcanic and Geothermal Earthquakes

Observations from dense local seismic networks show that earthquakes in volcanic areas commonly have non-DC mechanisms. In many cases, the data have been subjected to careful analysis, including waveform modeling (e.g., Dreger et al. 2000; Julian and Sipkin 1985), corrections for wave propagation through three-dimensional crustal structure determined from tomography (e.g., Miller et al. 1998a; Ross et al. 1996), and the use of multiple seismic phases. The clearest cases are from Iceland, California, and Japan.

Three volcano-geothermal areas on the spreading plate boundary in Iceland are rich sources of short-period, non-DC earthquakes. These are the Reykjanes, Hengill-Grensdalur, and Krafla volcanic-geothermal systems. At all three areas, small earthquakes occur that have unequal dilatational and compressional areas on the focal sphere, suggestive of isotropic components in their mechanisms. The non-DC earthquakes are intermingled spatially with DC events, indicating that the non-DC mechanisms are not artifacts of instrumental errors or propagation through heterogeneous structures.

The Hengill-Grensdalur triple junction is the best studied of these areas. It was there that experiments were first performed in sufficient detail to demonstrate beyond reasonable doubt that non-DC earthquakes with net volume changes occur in nature (Foulger 1988; Miller 1998a) (Fig. 9). The area is currently the richest source of extreme non-DC earthquakes known. Approximately 70 % of the earthquakes involve volume increases, i.e., their radiation patterns are dominated by compressions, and they are thought to be caused by thermal contraction in the heat source of the geothermal area (Fig. 10). The source mechanisms require more than simple tensile cracking, because the radiation patterns include both compressions and dilatations. Fluid flow and/or shear faulting probably also contribute components.

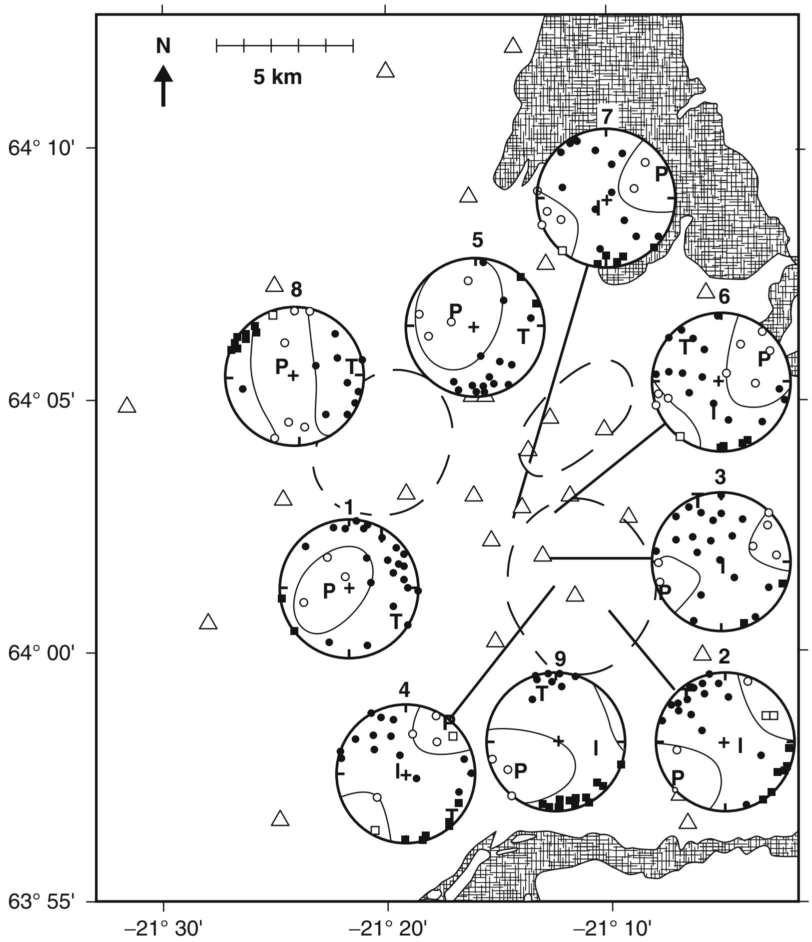

Fig. 9 Map of the Hengill-Grensdalur volcanic complex, Iceland, showing focal mechanisms of nine representative earthquakes. Events *5*, *6*, *8*, and *9* are indistinguishable from DCs. Compressional-wave polarities (*solid circles* indicate compressions; *open circles* indicate dilatations) and *P*-wave nodes are shown in upper focal hemisphere equal area projection. *Squares* denote downgoing rays plotted on the upper hemisphere. *T*, *I*, and *P* are positions of principal axes. *Lines* indicate epicentral locations. Where *lines* are absent, mechanisms are centered on epicenters. *Triangles* indicate seismometer locations; *dashed lines* show outlines of the main volcanic centers

Non-DC geothermal earthquakes with volumetric mechanisms occur also at several volcanic-geothermal areas in California, including the Geysers steam field (Ross et al. 1996), the Coso Hot Springs (Julian et al. 2010), and Long Valley caldera (Foulger et al. 2004). Industrial steam extraction and water reinjection at the Geysers induces thousands of small earthquakes per month in the reservoir. The mechanisms are typically closer to DCs than those of Icelandic geothermal earthquakes, and the volumetric non-DC components range from explosive to implosive, with approximately equal numbers of each type.

Non-DC earthquake focal mechanisms were observed at the Coso Hot Springs geothermal field, California, in March 2005. There, a fluid injection activated a fault plane on which earthquakes with non-DC mechanisms of uniform type occurred. These involved volume increases. The orientation of the mechanisms relative to the fault plane implied a process dominated by tensile failure with subsidiary shear faulting.

Abundant non-DC earthquakes were observed in a detailed experiment at Long Valley caldera in 1997. More than 80 % of the mechanisms had explosive volumetric components and most had compensated

Encyclopedia of Earthquake Engineering
DOI 10.1007/978-3-642-36197-5_290-1

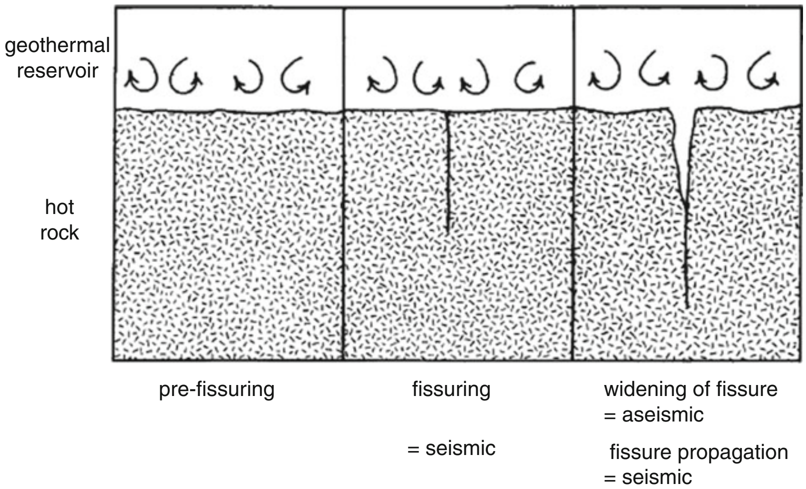

Fig. 10 Schematic illustration of seismogenic tensile cracking by thermal stresses caused by convective cooling of rocks at the heat source of a geothermal system (From Foulger 1988)

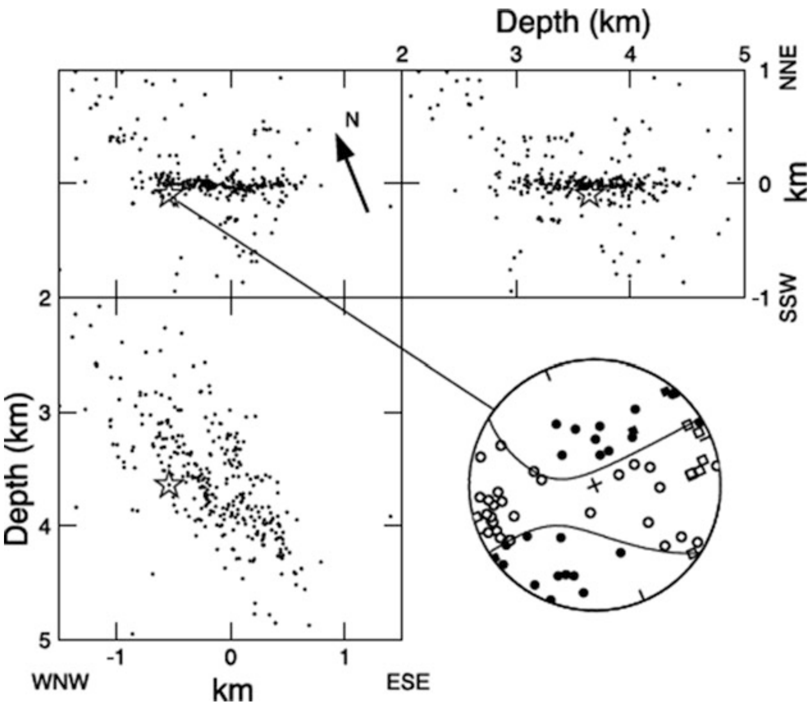

Fig. 11 Non-shear fault plane delineated by earthquake hypocenters. Views from three orthogonal directions showing the locations of 314 earthquakes (*black dots*) that lie between 2 and 5 km depth. *Upper left*: map view; *upper right*: SSW-NNE vertical cross-section; *lower left*: WNW-ESE vertical cross-section. *Star*: earthquake whose focal mechanism is shown at *lower right* as an upper-hemisphere plot of compressional-wave polarities. The mechanism for this earthquake is compatible with compensated tensile failure

linear-vector dipole components with outward-directed major dipoles. The simplest interpretation of these mechanisms is combined shear and extensional faulting accompanied by a volume-compensating process such as the rapid flow of water, steam, or CO_2 into opening tensile cracks A particularly well-recorded swarm was consistent with extensional faulting on an ESE-striking subvertical plane, an orientation

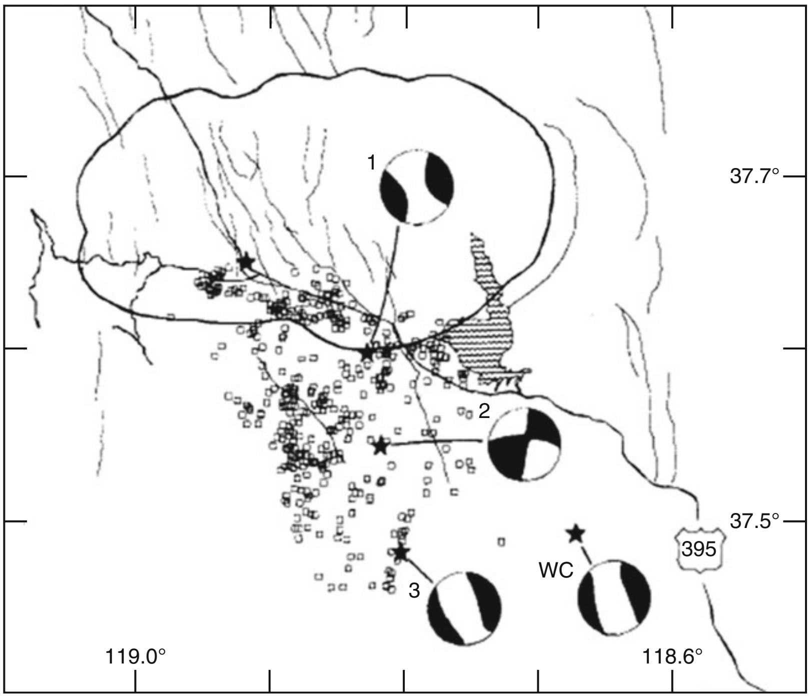

Fig. 12 Long Valley caldera, California, and vicinity, showing the best located earthquakes in 1980 and mechanisms for the largest earthquakes of 1978 and 1980 as lower-hemisphere, equal-area projections, with fields of compressional-wave polarity in *black*

consistent with the activated zone defined by the earthquake hypocenters. The orientations of non-DC earthquakes beneath Mammoth Mountain, a volcanic cone on the southwestern caldera rim, varied systematically with location, reflecting a variable local stress field. Events in a spasmodic burst indicated nearly pure compensated tensile failure and high fluid mobility (Foulger et al. 2004) (Fig. 11). Earthquakes with M_W 4.6–4.9 observed at regional distances on broadband sensors also had non-DC moment tensors with significant volumetric components and were probably caused by hydrothermal or magmatic processes (Dreger et al. 2000).

Earthquakes with non-DC radiation patterns, some of them moderately large, accompany magmatic and volcanic activity. Many non-DC earthquakes with *P*-wave polarities that are either all dilatational or all compressional accompanied the 1983 eruption of Miyakejima volcano, Japan. The earthquakes radiated significant shear waves, indicating that their mechanisms were not purely isotropic. The *P*-wave polarities and *P*- and *SV*-wave amplitudes are compatible with combined tensile and shear faulting (section "Combined Tensile and Shear Faulting"), an interpretation supported by the numerous open cracks that formed prior to the eruption. A similar but substantially larger earthquake, of magnitude 3.2, occurred 10 km beneath the Unzen volcanic region, western Kyushu, in 1987 (Shimizu et al. 1987).

Long Valley caldera, in eastern California, has experienced some of the largest clearly non-DC volcanic earthquakes. Four events with M_L greater than six occurred there in May 1980 (Fig. 12), and at least two had non-DC mechanisms. These events followed 2 years of volcanic unrest characterized by escalating seismic activity and surface deformation indicating magma-chamber inflation. Moment tensor inversions of different subsets of the available data conducted independently and using different methods all gave mechanisms that were similar and close to CLVDs. Any volumetric components were unresolvably small. The source processes probably involved tensile faulting at high fluid pressure, perhaps associated with dike intrusion. A M_S 5.6 earthquake similar in mechanism to the Long Valley earthquakes, though differently orientated, occurred near Tori Shima island, in the Izu-Bonin arc, on June 13, 1984. Because

DOI 10.1007/978-3-642-36197-5_290-1

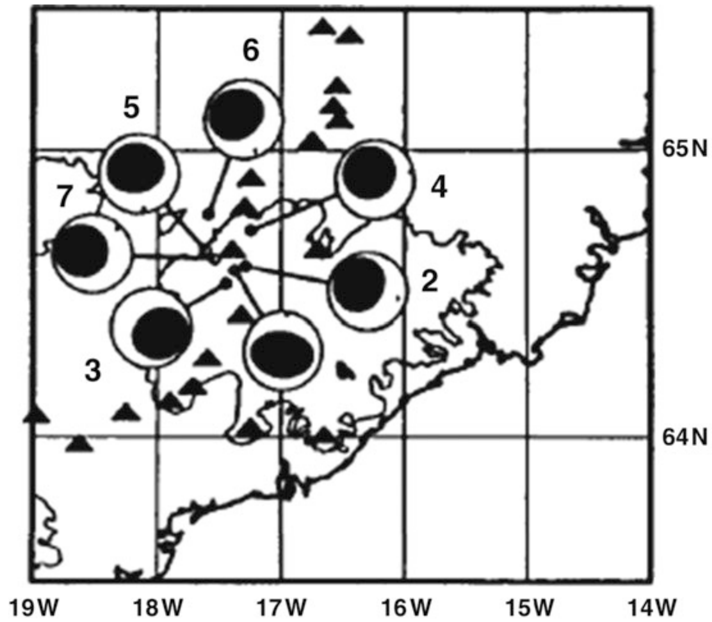

Fig. 13 Harvard centroid moment tensor mechanisms of earthquakes at Bardarbunga volcano, southeast Iceland, from Ekström (1994)

the earthquake was shallow, its full moment tensor could not be determined well, but the data were consistent with a mechanism close to a CLVD with a vertical symmetry axis. The seismic moment and source duration required intrusion of approximately 0.02 km^3 within 10–40 s (Kanamori et al. 1993).

Bardarbunga volcano, beneath the Vatnajökull ice cap in Iceland, regularly generates non-DC earthquakes with M_W 5.2–5.6 ($M_0 = 8$ to 30×10^{16} Nm) (Ekström 1994). They typically have nearly vertical CLVD-like mechanisms. A particularly well-studied example that occurred in 1996 yielded a non-DC mechanism with a 67 % vertically oriented compensated linear vector dipole component, a 32 % DC component, and a statistically insignificant (2 %) volumetric contraction. They may result from slip on a ring fault and can be explained by activation of less than 55° of such a fault. Cone sheets, which dip inward, have the most favorable geometry (Fig. 13).

Earthquakes at Mines

Deep mine excavations perturb the stresses in the surrounding rocks, reducing some components from values initially of the order of 100 MPa practically to zero. The resulting stress differences can exceed the strength of competent rock and cause earthquakes (often called "rock bursts," "coal bumps," etc.). Seismic data show clearly that many earthquakes at mines have non-DC mechanisms, usually with predominantly dilatational radiation patterns, that are incompatible with shear faulting.

An M_L 3.5 earthquake on May 14, 1981, at the Gentry Mountain mine, Utah, coincided with the collapse of a large cavity at 200-m depth in the mine.

Well-recorded earthquakes occurring at the Coeur d'Alene mining district, Idaho, had dilatational *P*-wave polarities, consistent with cavity collapse.

A M_W 3.9 event occurred in the Crandall Canyon coal mine, Utah, August 6, 2007, in association with a gallery collapse that killed six miners and, later, three rescuers. Its focal mechanism is dominated by an implosive component, consistent with a shallow underground collapse (Dreger et al. 2008).

Many non-DC earthquakes occurred in association with the excavation of a 3.5-m-wide tunnel in unfractured, homogeneous granite at the Underground Research Laboratory in Manitoba, Canada (Feignier and Young 1992). Moment tensors computed for 33 earthquakes with M_W −2 to −4 include

Encyclopedia of Earthquake Engineering
DOI 10.1007/978-3-642-36197-5_290-1

tensile, implosive, and shear mechanisms. Some were associated with breakout on the tunnel roof, and others occurred ahead of the active face.

Earthquakes located within 150 m of deep gold mines in the Witwatersrand, South Africa, had large volume decreases consistent with the partial collapse of mine galleries (McGarr 1992).

Fluid Injection

Fluids are injected into the shallow crust increasingly often for reasons such as increasing permeability within geothermal and hydrocarbon reservoirs by hydrofracturing, sequestration of CO_2, storing gas, and disposing of waste. Such injection often induces earthquakes, but they are not always monitored in detail. Nevertheless, in a number of well-studied cases non-DC source mechanisms have been observed (e.g., Baig and Urbancic 2010; Julian et al. 2010). Source types typically range from explosive to implosive dipoles. As underground fluid injections increase in importance over the coming decades, more detailed studies of the source mechanisms of the earthquakes induced may prove to be important for understanding the response of the Earth to such operations, project optimization and hazard mitigation.

Other Shallow Earthquakes

Real fault surfaces are not perfectly planar, and earthquakes on curved faults can, for some geometries, have non-DC mechanisms (Frohlich et al. 1989). Effects of this sort may account for the non-DC components observed in some large earthquakes, such as the 28-km deep M_S 7.8 event that occurred near Taiwan on November 14, 1986 (Zheng et al. 1995). The focal mechanism is inconsistent with shear faulting, but requires an implosive component. A similar, M 4.6 earthquake that occurred February 10, 1987, beneath the Kanto district, Japan. It had primarily dilatational compressional-wave polarities and was consistent with a conical nodal plane.

Deep-Focus Earthquakes

Earthquakes up to 700 hundred km deep occur in the mantle beneath subduction zones. The physical causes of deep earthquakes are not well understood. This is because minerals are expected to flow plastically at depths greater than about 30 km in normal areas. Processes that have been suggested to explain deep earthquakes include plastic instabilities, shear-induced melting, polymorphic phase transformations, and transformational faulting. Focal mechanisms can potentially shed light on this problem.

Volume changes in deep earthquakes are statistically unresolvable (less than 10 % of the seismic moment) (Kawakatsu 1991), indicating that polymorphic phase changes (section "Rapid Polymorphic Phase Changes"), play an insignificant role in deep earthquakes. Deep earthquakes do, however, have larger CLVD components than shallow earthquakes, and in some cases the sizes of the CLVD components increases systematically with depth and magnitude. The lack of large volume changes in deep earthquakes is compatible with complex shear faulting, and detailed waveform analysis resolves some deep non-DC earthquakes into DC subevents.

Glacial Earthquakes

Glaciers are subject to several kinds of sudden transient phenomena, apparently caused by diverse physical processes. Application of seismological analysis techniques to these events promises to provide fundamentally new types of data bearing on glacier dynamics and on understanding glaciers' response to influences such as climate change (Ekström et al. 2006).

Earthquakes apparently caused by glacier surges or calving, even though they can be large ($M \geq 4.5$), were recognized on seismograms only recently, because they have source durations of the order of a minute or more and excite high-frequency seismic waves only weakly. The application of arrayprocessing techniques to digital seismic data from the global network now enables us to detect dozens of large glacial earthquakes per year that previously went unnoticed. A particularly well-recorded event, of magnitude about 5, occurred in 1999 near the Dall glacier in the Denali range of Alaska, within a regional seismometer network and near a second, temporarily deployed, network. The low-frequency (~0.01–0.2 Hz) seismic waves are inconsistent with any moment-tensor mechanism, but agree well with those predicted for an approximately horizontal force directed in the direction of the glacier flow (Ekström et al. 2003). Seismic data from numerous other events, most of them near the margins of the Greenland icecap, are consistent with similar single-force mechanisms.

Most small ($M \geq -2.5$) icequakes in mountain glaciers have mechanisms describable by moment tensors, but they often differ greatly from DCs. Walter et al. (2009, 2010) recorded tens of thousands of events on Gornergletscher, in the Swiss Alps, on dense seismometer networks, and extended Dreger's waveform-inversion method, originally developed for earthquakes above magnitude 4, to frequencies approaching 1 KHz, in order to study the mechanisms of these microearthquakes. Most events had large explosive volumetric components, with source types close to those for opening tensile cracks. These included shallow events, probably representing crevasse opening, and events 100 m below the surface. Many shallow events were of a different type, equivalent to a DC combined with a volume decrease. A later study (Walter et al. 2010) of events near the base of the glacier found opening-crack mechanisms, but with inferred crack planes oriented horizontally.

Summary

A wide variety of processes can cause earthquake mechanisms to depart from the ideal DC force system that characterizes planar shear faulting in a homogeneous isotropic medium. These departures can be as extreme as unbalanced forces or torques associated with major landslides, glacial surges, or volcanic eruptions, or can be minor anomalies that are barely resolvable with the best data currently available. Studying non-DC earthquake mechanisms can be valuable for refining our knowledge of how faults work, for learning to understand and predict volcanic activity, for prospecting and exploiting geothermal energy and hydrocarbons, and for avoiding damage to civil and industrial infrastructure. Moreover, non-DC mechanisms are of direct value for monitoring mining and other industrial activities, particularly ones that involve fluid injection.

References

Aki K, Richards PG (2002) Quantitative seismology, 2nd edn. University Science, Sausalito
Anderson EM (1936) The dynamics of the formation of cone-sheets, ring-dykes, and cauldron-subsidences. Proc R Soc Edinb 56:128–156
Backus G (1977) Interpreting the seismic glut moments of total degree two or less. Geophys J R Astron Soc 51:1–25
Baig A, Urbancic T (2010) Microseismic moment tensors: a path to understanding frac growth. Lead Edge 29:320–324
Booth DC, Crampin S (1985) Shear-wave polarizations on a curved wavefront at an isotropic free surface. Geophys J R Astron Soc 83:31–45
Brace WF, Paulding BW Jr, Scholz CH (1966) Dilatancy in the fracture of crystalline rocks. J Geophys Res 71:3939–3953

DOI 10.1007/978-3-642-36197-5_290-1

Dreger DS, Tkalčić H, Johnston M (2000) Dilational processes accompanying earthquakes in the Long Valley caldera. Science 288:122–125

Dreger D, Ford SR, Walter WR (2008) Source analysis of the Crandall Canyon, Utah mine collapse. Science 321:217

Ekström G (1994) Anomalous earthquakes on volcano ring-fault structures. Earth Planet Sci Lett 128:707–712

Ekström G, Nettles M, Abers GA (2003) Glacial earthquakes. Science 302:622–624

Ekström G, Nettles M, Tsai VC (2006) Seasonality and increasing frequency of Greenland Glacial earthquakes. Science 311:1756–1758

Feignier B, Young RP (1992) Moment tensor inversion of induced microseismic events: evidence of non-shear failures in the $-4 < M < -2$ moment magnitude range. Geophys Res Lett 19:1503–1506

Foulger GR (1988) Hengill triple junction, SW Iceland; 2. Anomalous earthquake focal mechanisms and implications for process within the geothermal reservoir and at accretionary plate boundaries. J Geophys Res 93:13507–13523

Foulger GR, Julian BR, Hill DP, Pitt AM, Malin P, Shalev E (2004) Non-double-couple microearthquakes at Long Valley caldera, California, provide evidence for hydraulic fracturing. J Volcanol Geotherm Res 132:45–71

Frohlich C, Riedesel MA, Apperson KD (1989) Note concerning possible mechanisms for non-double-couple earthquake sources. Geophys Res Lett 16:523–526

Gajewski D (1993) Radiation from point sources in general anisotropic media. Geophys J Int 113:299–317

Gilbert F (1970) Excitation of the normal modes of the Earth by earthquake sources. Geophys J R Astron Soc 22:223–226

Hudson JA, Pearce RG, Rogers RM (1989) Source type plot for inversion of the moment tensor. J Geophys Res 94:765–774

Iguchi M (1994) A vertical expansion source model for the mechanisms of earthquakes originated in the magma conduit of an andesitic volcano: Sakurajima, Japan. Bull Volcanol Soc Jpn 39:49–67

Julian BR (1986) Analysing seismic-source mechanisms by linear-programming methods. Geophys J R Astron Soc 84:431–443

Julian BR (1994) Volcanic tremor: nonlinear excitation by fluid flow. J Geophys Res 99:11859–11877

Julian BR, Foulger GR (1996) Earthquake mechanisms from linear-programming inversion of seismic-wave amplitude ratios. Bull Seismol Soc Am 86:972–980

Julian BR, Sipkin SA (1985) Earthquake processes in the Long Valley caldera area, California. J Geophys Res 90:11155–11169

Julian BR, Foulger GR, Monastero FC, Bjornstad S (2010) Imaging hydraulic fractures in a geothermal reservoir. Geophys Res Lett 37:L07305. doi:10.1029/2009GL040933

Kanamori H, Given JW, Lay T (1984) Analysis of seismic body waves excited by the Mount St. Helens eruption of May 18, 1980. J Geophys Res 89:1856–1866

Kanamori H, Ekström G, Dziewonski A, Barker JS, Sipkin SA (1993) Seismic radiation by magma injection – an anomalous seismic event near Tori Shima, Japan. J Geophys Res 98:6511–6522

Kawakatsu H (1991) Insignificant isotropic component in the moment tensor of deep earthquakes. Nature 351:50–53

Knopoff L, Randall MJ (1970) The compensated linear vector dipole: a possible mechanism for deep earthquakes. J Geophys Res 75:4957–4963

McGarr A (1992) Moment tensors of ten Witwatersrand mine tremors. Pure Appl Geophys 139:781–800

Mendiguren JA (1977) Inversion of surface wave data in source mechanism studies. J Geophys Res 82:889–894

DOI 10.1007/978-3-642-36197-5_290-1

Miller AD, Julian BR, Foulger GR (1998a) Three-dimensional seismic structure and moment tensors of non-double-couple earthquakes at the Hengill-Grensdalur volcanic complex, Iceland. Geophys J Int 133:309–325

Miller AD, Foulger GR, Julian BR (1998b) Non-double-couple earthquakes II. Observations. Rev Geophys 36:551–568

Price NJ (1966) Fault and joint development in brittle and semi-brittle rock. Pergammon Press, New York

Richards PG, Kim WY, (2005) Equivalent volume sources for explosions at depth: Theory and observations. Bull Seismol Soc Am 95:401–407

Ross A, Foulger GR, Julian BR (1996) Non-double-couple earthquake mechanisms at The Geysers geothermal area, California. Geophys Res Lett 23:877–880

Shimizu H, Ueki S, Koyama J (1987) A tensile-shear crack model for the mechanism of volcanic earthquakes. Tectonophysics 144:287–300

Sipkin SA (1982) Estimation of earthquake source parameters by the inversion of waveform data: synthetic waveforms. Phys Earth Planet Inter 30:242–259

Takei Y, Kumazawa M (1994) Why have the single force and torque been excluded from seismic source models? Geophys J Int 118:20–30

Uhira K, Takeo M (1994) The source of explosive eruptions of Sakurajima volcano, Japan. J Geophys Res 99:17775–17789

Vavryčuk V (2005) Focal mechanisms in anisotropic media. Geophys J Int 161:334–346

Walter F, Clinton JF, Deichmann N, Dreger DS, Minson SE, Funk M (2009) Moment tensor inversions of icequakes on Gornergletscher, Switzerland. Bull Seismol Soc Am 99:852–870

Walter F, Dreger DS, Clinton JF, Deichmann N, Funk M (2010) Evidence for near-horizontal tensile faulting at the base of Gornergletscher, a Swiss Alpine glacier. Bull Seismol Soc Am 100:458–472

Woodhouse JH (1981) The excitation of long period seismic waves by a source spanning a structural discontinuity. Geophys Res Lett 8:1129–1131

Zheng T, Yao Z, Liu P (1995) The 14 November 1986 Taiwan earthquake – an event with isotropic component. Phys Earth Planet Inter 91:285–298